Physics of Fluids

Linear analysis on the interfacial instability of a spherical liquid droplet subject to a radial vibration

Cite as: Phys. Fluids **30**, 102104 (2018); https://doi.org/10.1063/1.5050517
Submitted: 31 July 2018 . Accepted: 03 October 2018 . Published Online: 24 October 2018

Yikai Li, Peng Zhang, and Ning Kang

View Online Export Citation CrossMark

ARTICLES YOU MAY BE INTERESTED IN

Effect of depth on the properties of two coupled Faraday waves in a Hele-Shaw cell
Physics of Fluids **30**, 102103 (2018); https://doi.org/10.1063/1.5054047

Pressure of a viscous droplet squeezing through a short circular constriction: An analytical model
Physics of Fluids **30**, 102004 (2018); https://doi.org/10.1063/1.5045495

Collaboration and competition between Richtmyer-Meshkov instability and Rayleigh-Taylor instability
Physics of Fluids **30**, 102105 (2018); https://doi.org/10.1063/1.5049869

AIP Publishing

© 2018 Author(s).

Linear analysis on the interfacial instability of a spherical liquid droplet subject to a radial vibration

Yikai Li,[1,a)] Peng Zhang,[2,a)] and Ning Kang[1]
[1]*School of Mechanical Engineering, Beijing Institute of Technology, Beijing 100081, China*
[2]*Department of Mechanical Engineering, The Hong Kong Polytechnic University, Hung Hom, Kowloon, Hong Kong*

(Received 31 July 2018; accepted 3 October 2018; published online 24 October 2018)

Precursory surface standing waves for liquid atomization occur on a spherical droplet subjected to a radial time-periodic force. In this paper, we carried out a linear stability analysis on the spherical Faraday instability. With the Floquet analysis, a derived difference equation gives the dispersion relation between the Floquet exponent and the spherical modes. For inviscid instability, the problem can also be reduced to the standard Mathieu equation as the same as its planar counterpart, but the parameters in the equation correspond to different quantities due to the spherical configuration. The analysis shows that increasing the density ratio of the ambient fluid to the droplet narrows the range of possibly excited spherical modes under the same forcing condition. For viscous instability, an additional parameter corresponding to the viscous effects was introduced into the difference equation. With increasing the droplet viscosity, the surface waves with large mode numbers are stabilized and hence a larger forcing amplitude is required to cause instability. Furthermore, the most-unstable spherical mode of the largest growth rate excited in the experimental condition is determined and discussed for its physical interpretation for droplet atomization caused by Faraday instability. *Published by AIP Publishing.* https://doi.org/10.1063/1.5050517

I. INTRODUCTION

An instability takes place at the interface between two different fluids when a time-periodic acceleration is exerted perpendicularly to the interface. This phenomenon is referred to as the "Faraday instability" to honor Faraday[1] who first academically studied the pattern formation of the standing waves on the surface of a liquid lying on a vibrating plate (a comprehensive review can be found in Ref. 2). This problem has attracted much academic attention because it relates to various interesting physics, such as pattern selection on the liquid surface,[3–6] spatiotemporal chaos,[7–10] liquid atomization,[11–14] and even cellular structures in flames in an acoustic field.[15–17]

It was observed that the oscillating frequency of the excited surface waves (referred to as "Faraday waves") was either half[1] or equal to[18] that of the vibrating plate. This discrepancy between the observed excitation frequencies was finally explained by Benjamin and Ursell[19] who described the growth of the amplitude of the Faraday waves on the planar liquid surface by using a system of Mathieu equations with the linear and inviscid assumptions. In their theory, two non-dimensional parameters, both of which are functions of fluid properties, forcing conditions, and surface wave modes, comprise the ordinate and abscissa of an instability diagram on which discrete unstable tongues with different oscillating frequencies of surface waves are generated. The excitation and frequency of a surface wave mode depends on its corresponding location on the instability diagram.

Recognizing that the theory of Benjamin and Ursell cannot explain the experimental observations related to fluid viscosity, Eisenmenger[20] and Ciliberto and Gollub[21] proposed a phenomenological model in which a linear damping term is empirically added to the Mathieu equation to account for the effect of viscosity. To further study the viscous dissipation in Faraday instability, Kumar and Tuckerman[22] and Kumar[23] applied Floquet theory to the linearized Navier-Stokes equations and derived an eigenvalue problem for the vector of Fourier components. A threshold acceleration amplitude of the external forcing for the onset of instability was obtained and found to be consistent with the experimental results.[24,25]

Besides the planar liquid layer, the deformation and atomization occurring on curved or spherical interfaces are also of great interest.[26–31] Considering no external forces, Rayleigh[32] derived an expression for the free oscillation frequency of an inviscid spherical droplet that is slightly disturbed. Later, Chandrasekhar[33] studied viscous effects on droplet oscillation in the linear regime. The interfacial dynamics are of more interest when external forces are introduced onto the droplet. Terrones and Carrara[34] performed a linear analysis for the Rayleigh-Taylor instability on a spherical droplet under a constant radial acceleration. When the external force becomes oscillatory, the Faraday instability and related mechanisms emerge, which play very important roles in many application fields, such as the oscillation and atomization of a water drop placed on a vibrating plate,[35–39] the oscillation patterns of a levitated water drop subjected to sectorial acoustic

[a)]Authors to whom correspondence should be addressed: liyikai@bit.edu.cn and pengzhang.zhang@polyu.edu.hk

forces,[40] and the atomization of a liquid drop exposed on a piezoelectric substrate through which surface acoustic waves (SAW) travel.[41,42]

The Faraday instability on a spherical interface has different characteristics from that on a planar one. To display this difference and understand the oscillation and breakup process of a spherical droplet in a more generalized fashion, it is worth first conducting a linear stability analysis of the spherical Faraday instability, which, however, has not attracted sufficient attention until very recently. Ebo Adou and Tuckerman[43] theoretically studied the linearized Faraday instability on a spherical viscous liquid droplet by using Floquet analysis and obtained the instability diagram for inviscid and viscous droplets. Their analysis was mainly focused on the one-fluid problem and thus the influence of surrounding medium was ignored. Although they formulated the boundary conditions and differential equations for the two-fluid problem where the surrounding medium is another incompressible viscous fluid, they did not solve the equation. Furthermore, the study of Ebo Adou and Tuckerman[43] does not discuss its implications to the droplet atomization, which motivated the present study. Previous experimental results on the atomization aroused by Faraday instability have clearly identified the relationship (usually referred to as "Lang's equation"[13]) between the leading size of atomized droplets and the forcing frequency, which indicates the existence of a predominant wavelength growing with the largest rate.[11,13,35,44] However, the physical explanation of this relationship is not yet clear. In this paper, we also conducted a linear analysis of Faraday instability on a viscous spherical droplet, with the focus on the effects of the surrounding fluid density and the dynamics associated with the atomization event caused by Faraday instability. In particular, we determine the most-unstable spherical mode to be excited for a specified experimental condition in the droplet atomization aroused by Faraday instability and reinterpret Lang's equation based on the present theoretical results. Our formulation follows and extends that used by Chandrasekhar[33] for the Rayleigh-Taylor instability on a sphere.

The rest of this paper is organized as follows. In Sec. II, the mathematical formulations, including the governing equations and the derived dispersion relation between the growth rate and spherical mode numbers are given. The dynamics of Faraday instability for inviscid and viscous droplets are discussed in Secs. III and IV, respectively. In Sec. V, the most unstable mode for a given experimental condition is determined and its implications for droplet atomization caused by Faraday instability are discussed. Finally, the conclusions drawn from this paper are given in Sec. VI.

II. MATHEMATICAL FORMULATIONS

A. Physical model and governing equations

As shown in Fig. 1, a spherical droplet of a viscous and incompressible fluid is surrounded by a quiescent medium of an inviscid and incompressible fluid. The densities of the droplet and the surrounding fluid are ρ_1 and ρ_2, respectively ($\rho_1 > \rho_2$). The two fluids are immiscible and the surface tension coefficient α is assumed to be constant and uniform.

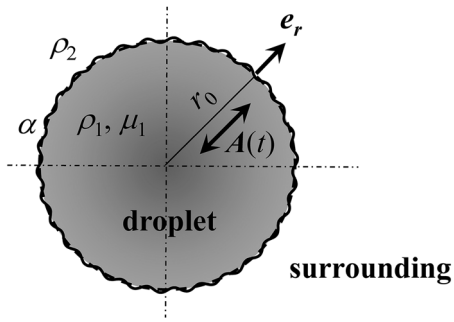

FIG. 1. Schematic of the spherical droplet of radius r_0 subjected to a radial periodic acceleration, $\boldsymbol{A}(t) = A_0 \cos(\Omega t)\boldsymbol{e}_\mathbf{r}$.

An acceleration evolving sinusoidally over time t with an angular frequency of Ω is imposed radially on the droplet and expressed by

$$\boldsymbol{A}(t) = A_0 \cos(\Omega t)\boldsymbol{e}_\mathbf{r}, \tag{1}$$

where A_0 is the acceleration amplitude and $\boldsymbol{e}_\mathbf{r}$ is the unit vector along the radial direction in the spherical coordinate system (r, θ, φ). The effect of gravitational acceleration, g, is neglected. This is justified if $A_0 \gg g$, which is generally satisfied in the liquid atomization caused by Faraday instability.

The governing equations for the incompressible viscous fluid motion inside the droplet are

$$\nabla \cdot \boldsymbol{u}_1 = 0, \tag{2}$$

$$\frac{\partial \boldsymbol{u}_1}{\partial t} + (\boldsymbol{u}_1 \cdot \nabla)\boldsymbol{u}_1 = -\frac{1}{\rho_1}\nabla p_1 + \nu_1 \nabla^2 \boldsymbol{u}_1 + \boldsymbol{A}, \tag{3}$$

where $\boldsymbol{u}_1$ is the velocity vector, p_1 is the pressure, and $\nu_1 = \mu_1/\rho_1$ is the kinematic viscosity. Since we neglect the viscous effects of the surrounding fluid ($\nu_2 = \mu_2/\rho_2 = 0$), the governing equations for the incompressible inviscid fluid motion outside the droplet are

$$\nabla \cdot \boldsymbol{u}_2 = 0, \tag{4}$$

$$\frac{\partial \boldsymbol{u}_2}{\partial t} + (\boldsymbol{u}_2 \cdot \nabla)\boldsymbol{u}_2 = -\frac{1}{\rho_2}\nabla p_2 + \boldsymbol{A}, \tag{5}$$

where $\boldsymbol{u}_2$ is the velocity vector and p_2 is the pressure.

The interface between the two fluids is defined by

$$F(r, \theta, \varphi, t) = r - [r_0 + \eta(\theta, \varphi, t)] = 0, \tag{6}$$

where θ and φ are the polar and azimuthal angle, r_0 is the initial radius of the droplet, and $\eta(\theta, \varphi, t)$ is the displacement disturbance on the droplet surface. The kinematic condition at the droplet surface is then given by

$$\frac{\partial F}{\partial t} + (\boldsymbol{u}_i \cdot \nabla)F = 0, \tag{7}$$

where $i = 1, 2$ for the fluid inside and outside the droplet, respectively. Substituting Eq. (6) into Eq. (7), we obtain

$$\frac{\partial \eta}{\partial t} + (\boldsymbol{u}_i \cdot \nabla)\eta = u_{ir}|_{r=r_0}, \tag{8}$$

where u_{ir} is the radial component of the velocity vector $\boldsymbol{u}_i$.

The dynamic condition at the droplet surface is obtained by considering the stress balance between the two fluids in both the normal and tangential directions. The normal stress balance equation gives

$$[\boldsymbol{n}\cdot\boldsymbol{\sigma}\cdot\boldsymbol{n}]_1^2 = \alpha\nabla\cdot\boldsymbol{n} = \alpha\left(\frac{1}{R_a}+\frac{1}{R_b}\right), \tag{9}$$

where $[x]_1^2 = x_2 - x_1$, $\boldsymbol{n} = \boldsymbol{e}_\mathbf{r}$ is the unit vector normal to the surface directing from fluid 1 to 2, $\boldsymbol{\sigma}$ is the stress tensor defined by

$$\boldsymbol{\sigma}_i = -p_i\boldsymbol{I} + \mu_i\left[\nabla\boldsymbol{u}_i + (\nabla\boldsymbol{u}_i)^T\right], \tag{10}$$

and R_a and R_b are the principle radii of curvature. The balance equation of tangential stress is given by

$$\left[\boldsymbol{n}\cdot\boldsymbol{\sigma}\cdot\boldsymbol{e_j}\right]_1^2 = 0, \tag{11}$$

where $\boldsymbol{e_j} = \boldsymbol{e_\theta}, \boldsymbol{e_\varphi}$ represent the unit vectors tangential to the droplet surface towards the polar and azimuthal directions, respectively.

The detailed procedures to linearize the governing equations and boundary conditions and the resultant solutions to the linearized problem are given in Appendixes A and B, respectively.

B. Dispersion relation

Using Eqs. (B11) and (B15) and the identity

$$\Delta_{\theta\varphi}Y_l^m = \nabla_H^2 Y_l^m = -l(l+1)Y_l^m, \tag{12}$$

where $Y_l^m(\theta,\varphi) = P_l^m(\cos\theta)e^{im\varphi}$ is the spherical harmonic, the normal stress balance condition (A9) reduces to

$$\sum_{l=0}^{+\infty}\sum_{m=0}^{l}\sum_{n=0}^{+\infty}\left\{\left[-\left(\frac{\rho_1}{l}+\frac{\rho_2}{l+1}\right)r_0\zeta_n^2 + 2\mu_1\zeta_n\frac{l-1}{lr_0}\frac{(2l+1)x - 2l(l+2)Q_{l+1/2}(x)}{2Q_{l+1/2}(x)-x} - \frac{\alpha(l-1)(l+2)}{r_0^2}\right]\eta_n + \frac{1}{2}(\rho_1-\rho_2)A_0(\eta_{n-1}+\eta_{n+1})\right\}e^{\zeta_n t}Y_l^m + (\rho_1-\rho_2)A_0\cos(\Omega t)r_0 + C_1(t) - C_2(t) - \frac{2\alpha}{r_0} = 0. \tag{13}$$

The coefficients of the Fourier term in Eq. (13) satisfy

$$\frac{1}{2}(\rho_1-\rho_2)A_0(\eta_{n-1}+\eta_{n+1}) = \left[\left(\frac{\rho_1}{l}+\frac{\rho_2}{l+1}\right)r_0\zeta_n^2 - 2\mu_1\zeta_n\frac{l-1}{lr_0}\frac{(2l+1)x-2l(l+2)Q_{l+1/2}(x)}{2Q_{l+1/2}(x)-x} + \frac{\alpha(l-1)(l+2)}{r_0^2}\right]\eta_n \tag{14}$$

since the spherical and Fourier modes are linearly independent. In addition, we can determine the integral constants C_1 and C_2 by

$$(\rho_1-\rho_2)A_0\cos(\Omega t)r_0 + C_1(t) - C_2(t) - \frac{2\alpha}{r_0} = 0 \tag{15}$$

along with an additional boundary condition of p_1 at $r = 0$.

The difference equation (14) gives the dispersion relation between the growth rate (real part of ζ_n) and the spherical modes (l) in a complicated fashion, which will be analyzed in detail in Secs. III and IV.

III. FARADAY INSTABILITY ON AN INVISCID DROPLET

A. Instability boundaries

To facilitate the following discussion and comparison with previous studies, we first consider an inviscid droplet, for which Eq. (14) reduces to the dimensionless form of

$$q(\eta_{n-1}+\eta_{n+1}) = \left(4\hat{\zeta}_n^2 + \lambda\right)\eta_n \tag{16}$$

with the definitions of

$$q = \frac{2(\rho_1-\rho_2)l(l+1)A_0}{[\rho_1(l+1)+\rho_2 l]r_0\Omega^2}, \quad \hat{\zeta}_n = \frac{\zeta_n}{\Omega}$$

and

$$\lambda = \frac{4\alpha(l-1)l(l+1)(l+2)}{[\rho_1(l+1)+\rho_2 l]r_0^3\Omega^2}. \tag{17}$$

Generally, we seek the real part of $\hat{\zeta}_n$ (growth rate) for a given composition of (q, λ), which can be understood as the dimensionless forcing acceleration and reciprocal of frequency, respectively, for specified fluids, droplet size, and spherical mode. Of particular interest in the present study is the neutral stable boundaries that are composed of a set of points (q, λ) rendering the growth rate $\beta = 0$. To determine the boundaries, we fix $\beta = 0$ and Eq. (16) reduces to

$$q\eta_{n-1} + 4(\hat{\gamma}+n)^2\eta_n + q\eta_{n+1} = \lambda\eta_n,\ n = 0,1,2,\ldots, \tag{18}$$

where $\hat{\gamma} = 0$ or 1/2 corresponding to the harmonic or subharmonic case, respectively. The reality condition requires $\eta_{-1} = \eta_1^*$ for $\hat{\gamma} = 0$ and $\eta_{-1} = \eta_0^*$ for $\hat{\gamma} = 1/2$,[22] where the quantity with the superscript * represents its conjugate form. For each value of q, λ can be determined by solving the positive eigenvalues of the coefficient matrix $\mathbf{M}$ of the difference equation (18). $\mathbf{M}$ is a real matrix of infinite dimensions. Typically, the eigenvalues of $\mathbf{M}$ are solved numerically by truncating it above a sufficiently large number N because the eigenvalues of lower orders of interest are converged as N increases.[45] The dimension of the truncated matrix is $(2N+2)\times(2N+2)$ because each component η_n contains real and imaginary parts.

Figure 2 shows the instability boundaries subdividing the λ-q plane into discrete regions. Only the first quadrant is displayed because $l \geq 1$ for the oscillatory spherical harmonics results in $\lambda \geq 0$ and $q > 0$ according to Eq. (17). In Fig. 2, the gray regions bounded by the neutral boundaries represent the unstable tongues, which intersect the λ-axis at k^2, where k is an integer. The initial disturbance modes corresponding to the parameter pairs (λ, q) located in these unstable tongues oscillate with the frequency of $k\Omega/2$ (k is an odd number for

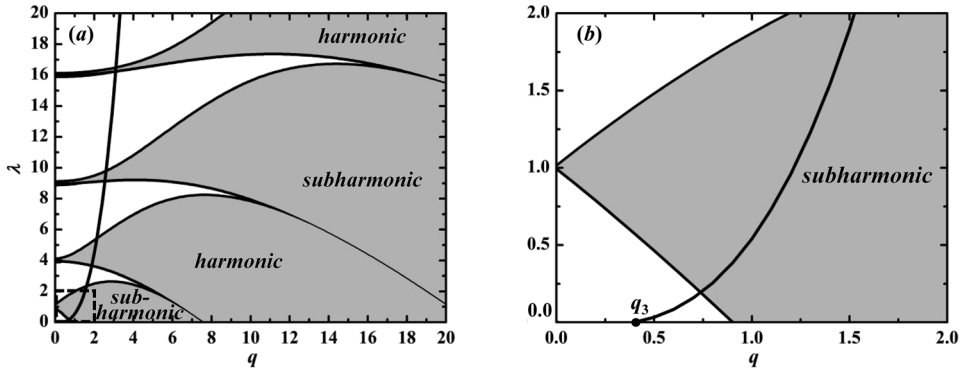

FIG. 2. Instability boundaries for the Faraday instability in the first quadrant of the λ-q plane. (a) The first four unstable tongues highlighted in gray. (*b*) Enlarged plot of the region bounded by the dashed rectangle in (a). The cubic curve intersecting the q-axis at q_3 represents all possible parameter pairs (λ, q) for a specified forcing condition $\Delta_0/r_0 = 0.2$ and $\alpha/\rho_1\Delta_0^3\Omega^2 = 1$ when $\rho_2 \to 0$. For each choice of Δ_0/r_0 and of $\alpha/\rho_1\Delta_0^3\Omega^2$, a cubic curve can be drawn in the λ-q plane like the one drawn in this figure.

subharmonic and even for harmonic) and grow to infinity as time elapses.

For the inviscid problem of spherical Faraday instability, there is no need to conduct the Floquet expansion on the time-dependent coefficient as done in Eq. (A13) because we do not solve the rotational component of the velocity [see Eqs. (B4) and (B5)]. As a result, instead of the recursion relation (16), the governing equation of the displacement disturbance η can be reduced to the Mathieu equation in the standard form of[19,43]

$$\frac{d^2\eta}{d\tilde{t}^2} + [\lambda - 2q\cos(2\tilde{t})]\eta = 0, \tag{19}$$

where $\tilde{t} \equiv \Omega t/2$ is a normalized time. The unstable tongues for Eq. (19) coincide with those shown in Fig. 2. The detailed procedures to derive the Mathieu equation can be found in Ref. 43.

From Fig. 2(a), it can be seen that the solution is unstable even for the case with an infinitesimal forcing acceleration amplitude A_0 (or q) if the forcing frequency Ω satisfies the condition (i.e., intersection points on the λ-axis)

$$\Omega = \frac{2}{k}\Omega_0, \quad k = 1, 2, \ldots, \tag{20}$$

where

$$\Omega_0 = \sqrt{\frac{\alpha(l-1)l(l+1)(l+2)}{[\rho_1(l+1)+\rho_2 l]r_0^3}} \tag{21}$$

is the free oscillating frequency of an inviscid droplet surrounded by another fluid for the spherical mode l.[32,46] Thus, Eq. (20) can be understood as the resonance condition in which the free oscillating frequency Ω_0 coincides with a subharmonic or harmonic of the radial forcing vibration.

B. Baseline instability modes

Before the detailed discussion on the influence of surrounding fluid density in Subsection III C and that of droplet viscosity in Sec. IV, we shall investigate the baseline case associated with the limit $\rho_2 \to 0$. Consequently, the parameter pair (λ, q) in Eq. (17) is reduced to

$$\lambda = \frac{4\alpha(l-1)l(l+2)}{\rho_1 r_0^3\Omega^2} \text{ and } q = \frac{2l\Delta_0}{r_0}, \tag{22}$$

which can be combined, by eliminating the spherical mode l, into an explicit expression of λ as a function of q as

$$\begin{aligned}\lambda &= \frac{\alpha}{2\rho_1\Delta_0^3\Omega^2}\left[q^3 + \frac{2\Delta_0}{r_0}q^2 - 8\left(\frac{\Delta_0}{r_0}\right)^2 q\right] \\ &= \frac{\alpha}{2\rho_1\Delta_0^3\Omega^2}q\left(q + \frac{4\Delta_0}{r_0}\right)\left(q - \frac{2\Delta_0}{r_0}\right),\end{aligned} \tag{23}$$

where Δ_0/r_0 and $\alpha/\rho_1\Delta_0^3\Omega^2$ are two dimensionless parameters usually predefined by a specified experimental condition (i.e., the size and properties of the droplet, forcing amplitude, and frequency). For each choice of Δ_0/r_0 and of $\alpha/\rho_1\Delta_0^3\Omega^2$, a cubic curve can be drawn in the λ-q plane as shown in Fig. 2, which intersects the q-axis at $q_1 = -4\Delta_0/r_0 < 0$, $q_2 = 0$, and $q_3 = 2\Delta_0/r_0 > 0$. Only the last intersection point q_3, denoted by a solid circle on the q-axis in Fig. 2(b), is physically meaningful in the present study since we must have $q > 0$.

The forcing accelerations are moderate in most practical experiments on the pattern selection and atomization induced by Faraday instability. As a result, the coefficient of the cubic term in Eq. (23), $\alpha/2\rho_1\Delta_0^3\Omega^2$, which represents the ratio of the surface tension force to the inertial force, is usually on the order of 10 or larger.[8,35,47] Moreover, the forcing displacement amplitude Δ_0 is typically much smaller than the droplet radius in these experiments and hence $q_3 = 2\Delta_0/r_0$ is significantly smaller than unity. Therefore, the cubic curve (23) for most practical experimental conditions originates from a small value on the q-axis and grows steeply over q (as shown in Fig. 5), and the q-values of interest for the unstable tongues of low orders are typically small.

For given values of Δ_0/r_0 and $\alpha/\rho_1\Delta_0^3\Omega^2$, all the parameter pairs (λ, q) corresponding to the possibly excited spherical modes ($l \geq 1$) are located along this curve and to the right of q_3 ($q = 2l\Delta_0/r_0 \geq 2\Delta_0/r_0 = q_3$). The droplet is unstable to the disturbance of the spherical mode l only if its corresponding parameter pair on this curve is inside the unstable tongues. Generally, the forcing displacement amplitude is far smaller than the radius of the droplet ($\Delta_0 \ll r_0$), which gives rise to a quite small value of q_3 close to the origin. This results in the excited spherical harmonics of relatively small modes (l) being located inside the first subharmonic unstable tongue.

C. Influence of surrounding fluid density

By comparing Eq. (17) with Eq. (22), we can see that the density of the surrounding fluid affects the parameter pair

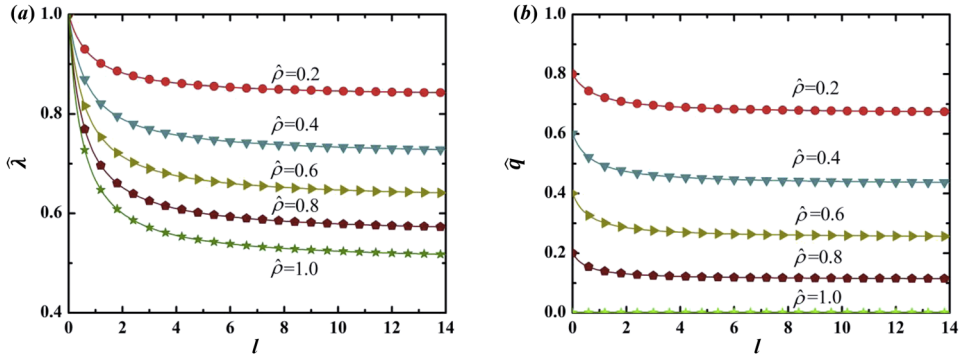

FIG. 3. Dependences of (*a*) $\hat{\lambda}$ and (*b*) $\hat{q}$ on the spherical mode l for different density ratios $\hat{\rho}$.

(λ, q) and in turn the possibly excited spherical modes for the same forcing condition (Δ_0, Ω) and fluid properties. We define the ratios of Eqs. (17)–(22) as

$$\hat{\lambda} = \frac{l+1}{(l+1)+\hat{\rho}l} \text{ and } \hat{q} = \frac{(1-\hat{\rho})(l+1)}{(l+1)+\hat{\rho}l}, \text{ where } \hat{\rho} = \rho_2/\rho_1, \tag{24}$$

to measure the effects of ρ_2 on the parameter pair (λ, q). In the present study, the density ratio $\hat{\rho}$ ranges from 0 to 1.

Figures 3(a) and 3(b) show the dependence of $\hat{\lambda}$ and $\hat{q}$ on the spherical mode l for different $\hat{\rho}$. As l increases, both $\hat{\lambda}$ and $\hat{q}$ monotonically decrease to constant limits

$$\hat{\lambda} \to \frac{1}{1+\hat{\rho}} \text{ and } \hat{q} \to \frac{1-\hat{\rho}}{1+\hat{\rho}}. \tag{25}$$

It is also noted that $\hat{\lambda}$ and $\hat{q}$ are sensitive to the variation of l only when l is small, say, $l < 2$. Thus, $\hat{\lambda}$ and $\hat{q}$ can be approximately treated as functions of $\hat{\rho}$ in the asymptotic form of Eq. (25) in the present study.

To study the effects of $\hat{\rho}$ on the possibly excited spherical modes, the parametric curves of λ and q, similar to that of Eq. (23), are drawn on the instability diagram for $\hat{\rho} = 0$, $\hat{\rho} = 0.4$, and $\hat{\rho} = 0.8$, as shown in Fig. 4. It is seen that, with increasing $\hat{\rho}$, the rapidly ascending parameter curve intersects with the q-axis at a smaller value and the line segments that are located in the unstable tongues shrink. This indicates that, for given fluid properties of the droplet and a specified forcing condition, increasing the density of the surrounding fluid tends to narrow and stabilize the possibly excited spherical modes due to Faraday instability.

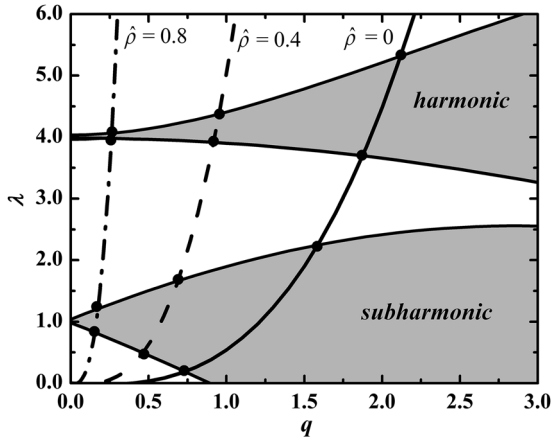

FIG. 4. Parametric curves for the cases of $\hat{\rho} = 0$ (solid curve), $\hat{\rho} = 0.4$ (dashed curve), and $\hat{\rho} = 0.8$ (dashed-dotted curve) with the same forcing condition and fluid properties inside the droplet on the instability diagram. Solid circles represent the points where the parametric curves intersect with the boundaries of unstable tongues.

IV. FARADAY INSTABILITY ON A VISCOUS DROPLET

A. Instability diagram

Considering the viscous effects of the droplet, Eq. (14) can be rewritten in the dimensionless form of

$$q(\eta_{n-1} + \eta_{n+1}) = \left(4\hat{\zeta}_n^2 + c\hat{\zeta}_n + \lambda\right)\eta_n \tag{26}$$

with the definitions of

$$c = 8\frac{\mu_1}{\Omega}\frac{l^2-1}{[\rho_1(l+1)+\rho_2 l]r_0^2}\frac{(2l+1)x - 2l(l+2)Q_{l+1/2}(x)}{x - 2Q_{l+1/2}(x)}, \tag{27}$$

in which the function Q can be simplified by considering the asymptotic expansion of the Bessel function $J_l(x)$ at $l \gg 1$,[48]

$$J_l(x) = \frac{e^l\left(\frac{1}{2}x\right)^l}{(2\pi l)^{1/2}l^l}\left[1 + O\left(l^{-1}\right)\right]. \tag{28}$$

Inserting Eq. (28) into the definition of $Q_l(x) = J_{l+1}(x)/J_l(x)$ leads to

$$\begin{aligned} Q_l(x) &\simeq \frac{e^{l+1}\left(\frac{1}{2}x\right)^{v+1}}{[2\pi(l+1)]^{1/2}(l+1)^{v+1}} \Big/ \frac{e^l\left(\frac{1}{2}x\right)^l}{(2\pi l)^{1/2}l^l} \\ &= \frac{ex}{2l}\sqrt{\frac{l}{l+1}}\left(\frac{l}{l+1}\right)^{l+1} \approx \frac{x}{2l}, \end{aligned} \tag{29}$$

with which the parameter c defined by Eq. (27) can be approximated as

$$c \simeq \frac{8\mu_1}{(\rho_1+\rho_2)\Omega}\left(\frac{l}{r_0}\right)^2 \tag{30}$$

at $l \gg 1$. For typical experiments associated with the wave pattern or atomization on a water drop surface caused by Faraday instability,[35,37,49] the magnitude of c is on the order of 0.1–1.

Following the same procedure to obtain the neutral instability boundaries for the inviscid case, we first set $\beta = 0$ and Eq. (26) reduces to

$$\begin{aligned} &q\eta_{n-1} + \left[4(\hat{\gamma}+n)^2 - c(\hat{\gamma}+n)i\right]\eta_n + q\eta_{n+1} \\ &\quad = \lambda\eta_n, \ n = 0, 1, 2, \ldots. \end{aligned} \tag{31}$$

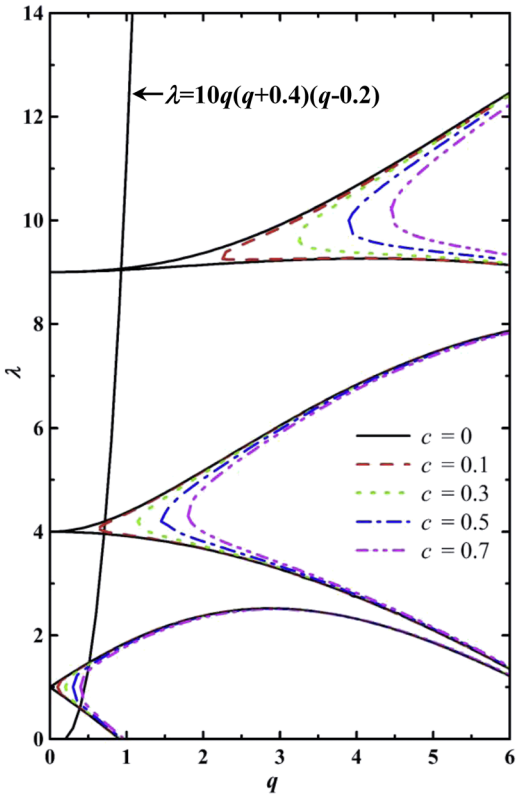

FIG. 5. Boundaries of the first three unstable tongues (k = 1, 2, 3) for c = 0 (black solid line), c = 0.1 (red dashed line), c = 0.3 (green dotted line), c = 0.5 (blue dashed-dotted line), and c = 0.7 (purple dashed-dotted-dotted line). The cubic curve is $\lambda = 10q(q + 0.4)(q - 0.2)$, representing one practical experimental condition in which $\alpha/2\rho_1\Delta_0^3\Omega^2 = 10$ and $\Delta_0/r_0 = 0.1$.

Consequently, for each given value of q, λ are the real positive eigenvalues of the coefficient matrix of the form

$$\mathbf{M} = \begin{pmatrix} 0 & 0 & 2q & 0 & 0 & 0 & \dots \\ 0 & 0 & 0 & 0 & 0 & 0 & \dots \\ q & 0 & 4 & c & q & 0 & \dots \\ 0 & q & -c & 4 & 0 & q & \dots \\ 0 & 0 & q & 0 & 16 & 2c & \dots \\ 0 & 0 & 0 & q & -2c & 16 & \dots \\ \vdots & \vdots & \vdots & \vdots & \vdots & \vdots & \dots \end{pmatrix} \tag{32}$$

for the subharmonic instability and

$$\mathbf{M} = \begin{pmatrix} 1+q & c/2 & q & 0 & 0 & 0 & \dots \\ -c/2 & 1-q & 0 & q & 0 & 0 & \dots \\ q & 0 & 9 & 3c/2 & q & 0 & \dots \\ 0 & q & -3c/2 & 9 & 0 & q & \dots \\ 0 & 0 & q & 0 & 25 & 5c/2 & \dots \\ 0 & 0 & 0 & q & -5c/2 & 25 & \dots \\ \vdots & \vdots & \vdots & \vdots & \vdots & \vdots & \dots \end{pmatrix} \tag{33}$$

for the harmonic instability. Solving the eigenvalue problem of Eqs. (32) and (33) gives the instability boundaries for different c-values in the q-λ plane as shown in Fig. 5.

B. Movement of unstable boundaries

As shown in Fig. 5, different from the inviscid case where the unstable tongues attach to the λ-axis at k^2, the unstable tongues for the viscous condition detach from the λ-axis.[50–52] With the increase of the c-value, the vertex of the unstable tongue moves away from the λ-axis while the area of the unstable tongue shrinks. In the present study focusing on the forcing vibration system, the q-value at the vertex of the kth unstable tongue, q_k, signifies the minimum forcing displacement amplitude (or forcing strength) required to cause instability. Thus, the outward displacement of q_k away from the λ-axis with the increase of c indicates that the threshold of forcing strength to destabilize the system is enhanced as the effect of viscosity rises.

TABLE I. Computed q_k-values by Eq. (31) with c = 0.1, 0.3, 0.5, and 0.7 (corresponding to the red dashed line, green dotted line, blue dashed-dotted line, and purple dashed-dotted-dotted line, respectively, in Fig. 5) for the first four unstable tongues (k = 1, 2, 3, 4).

	c = 0.1	c = 0.3	c = 0.5	c = 0.7
k = 1	0.1	0.2	0.3	0.4
k = 2	0.7	1.2	1.5	1.8
k = 3	2.2	3.3	3.9	4.5
k = 4	4.8	6.5	7.5	8.3

Table I shows the q_k-values computed numerically by Eq. (31) for the first four unstable tongues. Again, one can see that the unstable tongues of higher order k move further away (larger q_k-value) from the λ-axis for the same c-value. This means that it requires much larger forcing acceleration to excite the spherical modes located in the unstable tongues of higher orders. This is the reason why the subharmonic instability (k = 1) is always observed in most experiments since the first unstable tongue moves least from the λ-axis.

Another interesting behavior of the viscous case is that λ at the vertex of unstable tongues also varies with k and c. We define the λ-value at the vertex of the kth unstable tongue as $k^2 + \lambda_k$, where λ_k is tabulated in Table II for the first four unstable tongues with c = 0.1, 0.3, 0.5, and 0.7. λ_k physically represents the deviation of the resonant forcing frequency from the inviscid resonance condition (20) due to the viscous effect. The viscous resonance condition can hence be written as

$$\Omega(k, c) = \frac{2}{\sqrt{k^2 + \lambda_k}}\Omega_0, \quad k = 1, 2, 3, \dots. \tag{34}$$

From Fig. 5 and Table II, it can be seen that the magnitude of λ_k increases with c and k. Except the first unstable tongue, in which the resonant frequency is slightly larger than the

TABLE II. Computed λ_k-values by Eq. (31) with c = 0.1, 0.3, 0.5, and 0.7 (corresponding to the red dashed line, green dotted line, blue dashed-dotted line, and purple dashed-dotted-dotted line, respectively, in Fig. 5) for the first four unstable tongues (k = 1, 2, 3, 4).

	c = 0.1	c = 0.3	c = 0.5	c = 0.7
k = 1	−0.002	−0.005	−0.011	−0.020
k = 2	0.076	0.195	0.277	0.358
k = 3	0.309	0.680	0.917	1.162
k = 4	0.802	1.485	1.955	2.347

inviscid one, the resonant forcing frequency for the other unstable tongues decreases as the viscous effect increases.

C. Instability modes influenced by damping

The unstable tongues for the inviscid (undamped) case, as shown in Fig. 2, are fixed on the λ-q plane. All the possibly excited spherical modes for a given experimental condition are located on the line segments between the points where the parameter curves intersect with the boundaries of the same unstable tongues. In the phenomenological model[21] for the viscous case, in which the development of the surface displacement is governed by a damped Mathieu equation with a constant coefficient of the damping term, the unstable tongues are also fixed on the λ-q plane for a specified experimental condition and the unstable modes are determined similar to the undamped case. However, the rigorous analysis in the present study is more complicated for the viscous case because the unstable tongues are dependent on the parameter c, which is in turn a function of the spherical mode number. As a result, the ranges of unstable tongues are variable even for a predefined condition.

To study the effects of viscous damping on the unstable modes excited in the spherical Faraday instability for a specified forcing condition, two scenarios to vary the c-value are discussed as follows.

First, the droplet viscosity is varied and the spherical mode number is fixed. For a specified spherical mode l whose corresponding parameter pair (λ, q) on the parameter curve is inside an unstable tongue, increasing the droplet viscosity (or c-value) contracts the unstable tongue (as shown in Fig. 5) so that the parameter pair (λ, q) may be moved outside the unstable tongue when the viscosity exceeds a certain value. This scenario characterizes that increasing the viscosity could stabilize the spherical mode that is unstable for lower viscosities.

Second, the spherical mode number is varied. For a specified forcing condition, c-value is also variable depending on the spherical mode number l besides the liquid viscosity. In this case, to determine the droplet stability and the possibly excitable spherical modes under a given experimental condition, we need to first calculate (λ, q) and c by Eqs. (17) and (27) for each spherical mode and viscosity and then depict the unstable tongues for the c-value corresponding to the concerned mode and viscosity on the λ-q plane. If (λ, q) for the mode is located within one of the unstable tongues, the droplet is unstable for this particular mode. This process is repeated for different mode numbers and viscosities until all the excited spherical modes can be identified for this experimental condition. As discussed above, since the unstable tongues are contracted more severely for higher orders (i.e., higher k-values), the spherical modes with higher orders are less likely to be excited.

V. MOST UNSTABLE MODE AND ITS IMPLICATIONS FOR DROPLET ATOMIZATION

If the external forcing is sufficiently strong, the most-unstable surface waves on the droplet would dominate over other unstable waves and increase their amplitudes until their tips break up. This type of breakup has been employed in many industrial applications to realize liquid atomization,[11,13,53] in which the atomized children droplets are usually much smaller than the parent droplet. This indicates that the most-unstable spherical modes (with the largest growth rate) are substantially larger than unity. Consequently, it is of practical interest to analytically determine the most-unstable mode and its growth rate for a given experimental condition. It is noted that although the most-unstable mode is obtained in the frame of the linear theory which is valid only for the small surface deformation, the mode is still supposed to continue to lead in growth when the surface deformation becomes large.[54]

Figures 6(a) and 6(b) show the contour curves of different dimensionless growth rates $\hat{\beta}$ in the λ-q diagram for the inviscid fluids. These curves were obtained by numerically solving the eigenvalue problem (16) with different $\hat{\beta}$-values. From Fig. 6(a), we can see that the same dimensionless growth rate can exist in different orders of unstable tongues; however, the unstable tongues of higher order contain more contour curves of larger growth rates. The neutral unstable tongues (black curves) are in a shape of protruding to the left. With the increase of $\hat{\beta}$-value, the area of the unstable tongues shrinks and the left-most boundary is smoothed and retracts rightwards. The retraction distance for the same growth rate increases with the order of unstable tongues.

As discussed in Secs. II–IV, each realization of a specific experiment condition on the Faraday instability can be depicted as a cubic curve in the λ-q diagram depending on the dimensionless parameter $\hat{\alpha} = \alpha/\rho_1 \Delta_0^3 \Omega^2$. Figures 6(a) and 6(b) show these cubic curves for different $\hat{\alpha}$-values larger than $O(1)$, which are typical conditions adopted in the experiments on the surface pattern selection and atomization induced by Faraday instability.[6,35,37,47] It can be seen that the cubic curves for the typical experimental condition are steep. Due to

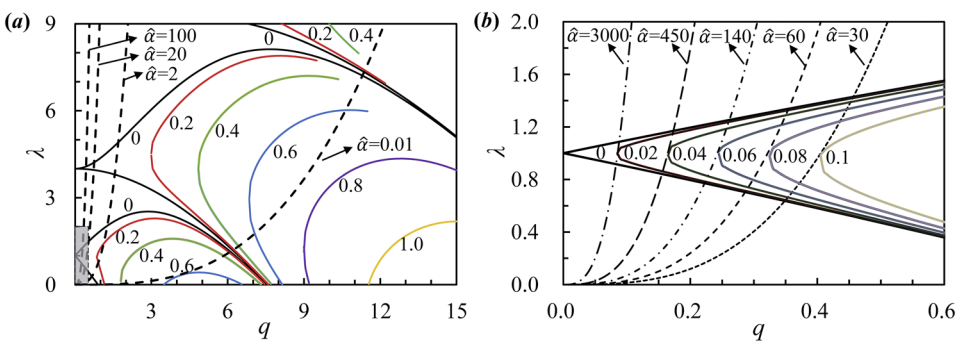

FIG. 6. Contour curves for different dimensionless growth rates $\hat{\beta}$. Each cubic curve represents one experimental realization with a specified value of $\hat{\alpha} = \alpha/\rho_1 \Delta_0^3 \Omega^2$. Panel (b) is the enlargement of the gray region near the origin of panel (a).

more retraction for the unstable tongues of the same growth rate in the higher order, the largest growth rate that the cubic curve passes through in the unstable tongues of the first order is larger than those of higher orders within the typical range of $\hat{\alpha}$-values in experiment. As a result, even for the inviscid case, the most-unstable modes are usually located in the first subharmonic region.

Figure 6(a) also shows a hypothetical case of $\hat{\alpha} = 0.01$, which is hardly realized in experiment. It is clear that the overall largest growth rate is located in the harmonic region (the unstable tongue of the second order), which indicates that the harmonic oscillation of the excited surface waves is realizable if the forcing acceleration is large enough. In other words, there exists a threshold value of $\hat{\alpha}$ for the transition of the excited surface waves from the subharmonic response to harmonic response.

It is well known that the leading size of the atomized droplets is proportional to the predominant surface wavelength.[47] In the study on the characteristics of atomization of a liquid layer under vertical vibration with the frequency in the ultrasonic range, Lang[13] found that the leading diameter of the atomized droplets decreases as the forcing frequency increases, which can be described by the so-called Lang's equation

$$d_c = (0.35 \pm 0.03)\Lambda_c = (0.35 \pm 0.03) \cdot 2\pi\left(\frac{\alpha}{\rho_1}\right)^{1/3}\left(\frac{2}{\Omega}\right)^{2/3}. \tag{35}$$

Although this equation has been validated by many subsequent experiments on both planar and spherical situations,[11,35,44] its physical explanation is unclear. In most of the previous studies, the second equality in Eq. (35), $\Lambda_c = 2\pi(\alpha/\rho_1)^{1/3}(2/\Omega)^{2/3}$, was explained as Kelvin's expression for the wavelength of the "forcing-free" surface wave oscillating at a frequency of $\Omega/2$,[55] which should be generally different from the predominant wavelength excited by vibration in the Faraday instability. Based on the present theoretical work, we can alternatively explain Eq. (35) as follows.

Recalling that the most-unstable mode occurs in the first subharmonic unstable region during most of the experimental range with $\hat{\alpha} > O(1)$, we show in Fig. 6(b) the enlargement of the region near the origin of Fig. 6(a). The most-unstable mode for each experimental realization is the point on the corresponding cubic curve that is tangent to one contour curve. Typically, this point is located around the left-protruding peak of the contour curves of the growth rate, whose ordinates λ are hardly varied from unity throughout most of the experimental conditions. Hence, by definition of $\Lambda = 2\pi r_0/l$ for the wavelength on a spherical surface, the predominant surface wavelength can be approximately expressed as

$$\Lambda_c = 2\pi r_0/l_c = 2\pi(\alpha/\rho_1)^{1/3}(2/\Omega)^{2/3} \tag{36}$$

if $l \gg 1$. Equation (36) coincides with Kelvin's expression and has clear physical meaning. In fact, if the forcing is further enhanced, the ordinate corresponding to the most-unstable mode may depart greatly from the straight line $\lambda = 1$, and thus Eq. (36) and Lang's equation (35) are no longer valid.

In our previous experimental study on the droplet atomization subject to a vertical vibration at a fixed frequency of 1.35 kHz with the voltage of the vibration signal ranging from 0 to 70 V,[38] the experimentally observed wavelength on the droplet surface is about 1.01 mm. Based on the present theory, the cubic curves for the cases studied in the experiments, whose corresponding $\hat{\alpha}$-values are on the order of $O(10)$–$O(100)$, intersect with their largest growth rate curves near the points $(1, q)$ (as shown in Fig. 6). Using the definition of $\lambda = 4\alpha(l-1)l(l+2)/\rho_1 r_0^3\Omega^2 = 1$, we can calculate that the predominant surface wavelength is about $2\pi r_0/l = 1.05$ mm, which agrees well with the experimental result.

It should be noted that, different from the continuous nature of the normal modes in the planar case, the mode numbers in the spherical Faraday instability are positive integers and hence discrete. However, the analysis shown above does not guarantee that the most-unstable spherical mode number l_c is an integer. Consequently, there may exist multiple discrete mode numbers having the same growth rate.[34]

VI. CONCLUDING REMARKS

In the present study, we have conducted a linear Faraday instability analysis on a viscous spherical droplet immersed in another inviscid fluid and subjected to a time-periodic radial acceleration. This analysis extends and supplements the previous studies by considering the effects of the density of the surrounding fluid and the practical implications of the most-unstable modes in liquid droplet atomization.

With the spherical harmonic decomposition in the θ and φ directions and with the Floquet decomposition in time, the linearized governing equations and corresponding boundary conditions constitute an eigenvalue problem. A difference equation is derived to give the dispersion relation between the Floquet exponent and the spherical modes.

For the inviscid case, solving the positive eigenvalues of the coefficient matrix $\mathbf{M}$ of the difference equation gives the neutral stable boundaries which subdivide the λ-q plane into discrete regions. The inviscid spherical Faraday instability can also be reduced to the Mathieu equation in the standard form. All the spherical modes in a specified forcing condition can be depicted as a cubic curve on this parameter plane. Only the modes on the line segments between the points where the cubic curve intersects with the boundaries of the unstable tongues are possibly excited. Furthermore, increasing the density of the fluid surrounding the droplet would narrow the range of possibly excited spherical modes. Therefore, the density of the surrounding fluid plays a stabilizing effect in Faraday instability.

The fluid viscosity causes an additional parameter c into the difference equation, which results in a different coefficient matrix from its inviscid counterpart. Solving the eigenvalues of the matrix gives unstable tongues for different c-values in the λ-q diagram. The viscous damping effect smoothens the unstable tongues while moving them away from the λ-axis. With the increase of the c-value, the unstable tongues contract their areas and retract farther from the λ-axis. This retraction is more deteriorated for the unstable tongues of higher order. As a result, the surface waves of large mode numbers become

stable and therefore a larger forcing amplitude is required to trigger instability of more viscous droplets. Moreover, the resonant forcing frequencies for the unstable tongues of orders larger than unity are decreased with increasing the viscous effect.

Motivated by identifying the most-unstable mode responsible for the leading size of atomized children droplets, we plotted contour curves for different growth rates in the λ-q diagram. We found that the most-unstable modes during common experimental conditions approximately satisfy the condition $\lambda = 1$, which coincides with Kelvin's expression, consequently reinterpreting Lang's equation. We found that once the external forcing is further enhanced beyond the common experiment condition, Lang's equation may become invalid and the most-unstable mode may be shifted to the harmonic unstable region.

ACKNOWLEDGMENTS

The work in the Beijing Institute of Technology was supported by the National Natural Science Foundation of China (Grant No. 51606010) and Beijing Natural Science Foundation (Grant No. 3174055). The work in the Hong Kong Polytechnic University was supported by the Hong Kong Research Grants Council/General Research Fund (PolyU 152217/14E and PolyU 152651/16E).

APPENDIX A: LINEARIZATION OF GOVERNING EQUATIONS

To conduct a linear analysis on the Faraday instability, we first linearize the governing equations described in Sec. II A about the state of rest (i.e., the unperturbed spherical droplet and the surrounding fluid are initially at rest with zero velocity), which leads to

$$\nabla \cdot \boldsymbol{u}_1 = 0, \tag{A1}$$

$$\frac{\partial \boldsymbol{u}_1}{\partial t} = -\frac{1}{\rho_1}\nabla p_1 + \nu_1 \nabla^2 \boldsymbol{u}_1 + \boldsymbol{A} \tag{A2}$$

and

$$\nabla \cdot \boldsymbol{u}_2 = 0, \tag{A3}$$

$$\frac{\partial \boldsymbol{u}_2}{\partial t} = -\frac{1}{\rho_2}\nabla p_2 + \boldsymbol{A}. \tag{A4}$$

In such a context, $\boldsymbol{u_i}$ and p_i represent the perturbation velocity and pressure, respectively.

Correspondingly, the kinematic condition Eq. (8) is linearized to

$$\frac{\partial \eta}{\partial t} = u_{1r}|_{r=r_0+\eta} = u_{2r}|_{r=r_0+\eta}. \tag{A5}$$

For the dynamic boundary condition in the normal direction, substituting Eq. (10) into Eq. (9) leads to

$$p_1|_{r=r_0+\eta} - p_2|_{r=r_0+\eta} = \alpha\left(\frac{1}{R_a}+\frac{1}{R_b}\right) + 2\mu_1 \left.\frac{\partial u_{1r}}{\partial r}\right|_{r=r_0+\eta}, \tag{A6}$$

in which the principle radii of curvature satisfy

$$\frac{1}{R_a}+\frac{1}{R_b} = \frac{2}{r_0} - \frac{1}{r_0^2}\left(2\eta + \nabla_H^2 \eta\right), \tag{A7}$$

up to the first order in η,[46] where

$$\nabla_H^2 \equiv \frac{1}{\sin\theta}\frac{\partial}{\partial\theta}\left(\sin\theta\frac{\partial}{\partial\theta}\right) + \frac{1}{\sin^2\theta}\frac{\partial^2}{\partial\varphi^2} \tag{A8}$$

is the horizontal spherical Laplacian operator. Substituting Eq. (A7) into Eq. (A6), we have the following linearized form of the pressure jump condition across the interface:

$$p_1|_{r=r_0+\eta} - p_2|_{r=r_0+\eta} = \frac{2\alpha}{r_0} - \frac{\alpha}{r_0^2}\left(2\eta + \nabla_H^2\eta\right) + 2\mu_1 \left.\frac{\partial u_{1r}}{\partial r}\right|_{r=r_0+\eta}. \tag{A9}$$

Because of the inviscid assumption of the fluid outside the droplet ($\mu_2 = 0$), the tangential stress balance equation Eq. (11) can be simplified as

$$\sigma_{r\theta} = \mu_1\left(\frac{1}{r}\frac{\partial u_{1r}}{\partial\theta} - \frac{u_{1\theta}}{r} + \frac{\partial u_{1\theta}}{\partial r}\right) = 0 \tag{A10}$$

and

$$\sigma_{r\varphi} = \mu_1\left(\frac{1}{r\sin\theta}\frac{\partial u_{1r}}{\partial\varphi} - \frac{u_{1\varphi}}{r} + \frac{\partial u_{1\varphi}}{\partial r}\right) = 0. \tag{A11}$$

The displacement disturbance on the droplet surface $\eta(\theta,\varphi,t)$ is expanded in series of spherical harmonics $Y_l^m(\theta,\varphi) = P_l^m(\cos\theta)e^{im\varphi}$ as

$$\eta(\theta,\varphi,t) = \sum_{l=1}^{+\infty}\sum_{m=-l}^{l}\eta_l^m(t)Y_l^m(\theta,\varphi), \tag{A12}$$

with the time-dependent coefficient written in the Floquet form,[22,23]

$$\eta_l^m(t) = e^{(\beta+i\gamma)t}\sum_n \eta_n(l,m)e^{in\Omega t} = \sum_n \eta_n(l,m)e^{\zeta_n t}, \tag{A13}$$

where $\beta + i\gamma$ is the Floquet exponent, η_n is the coefficient of Fourier mode n, and the real part of $\zeta_n \equiv \beta + i(\gamma + n\Omega)$, namely, β, can be considered as the growth rate. Equations (A1)–(A5) and (A9)–(A13) constitute the present eigenvalue problem to be solved in Appendix B.

APPENDIX B: SOLUTIONS TO THE LINEARIZED PROBLEM

With the identity $\nabla\times\nabla\times\boldsymbol{u}_1 = \nabla(\nabla\cdot\boldsymbol{u}_1) - \nabla^2\boldsymbol{u}_1$ and the continuity equation (A1), Eq. (A2) can be rewritten as

$$\frac{\partial \boldsymbol{u}_1}{\partial t} = -\frac{1}{\rho_1}\nabla p_1 - \nu_1\nabla^2\times\boldsymbol{u}_1 + \boldsymbol{A}. \tag{B1}$$

We decompose the velocity vector $\boldsymbol{u}_1$ into the irrotational component $\nabla\phi_1$ and the rotational component $\boldsymbol{\psi}_1$ as $\boldsymbol{u}_1 = \nabla\phi_1 + \boldsymbol{\psi}_1$, which satisfy

$$\nabla^2\phi_1 = 0, \tag{B2}$$

$$p_1 = -\rho_1\frac{\partial\phi_1}{\partial t} + \rho_1 A_0\cos(\Omega t)r + C_1(t), \tag{B3}$$

$$\nabla\cdot\boldsymbol{\psi}_1 = 0, \tag{B4}$$

$$\frac{\partial\boldsymbol{\psi}_1}{\partial t} + \nu_1\nabla^2\times\boldsymbol{\psi}_1 = 0, \tag{B5}$$

where $C_1(t)$ is an integral constant as a function of t. It can readily be shown by using tensor identities and integration that Eqs. (B2)–(B5) are equivalent to Eq. (B1) and the continuity equation.

For a given spherical harmonic $Y_l^m(\theta,\varphi)$, considering that ϕ_1 is finite at $r=0$, the general solution to Eq. (B2) is

$$\phi_1(r,\theta,\varphi,t)=\sum_n B_n e^{\zeta_n t} r^l Y_l^m(\theta,\varphi), \tag{B6}$$

where B_n is to be determined by applying the boundary conditions. Note that the indices (l,m) and corresponding sums for ϕ_1 and other similar quantities are omitted for mathematical conciseness. Equations (B4) and (B5) are solved by following the methodology proposed by Chandrasekhar[33] and the three components of $\boldsymbol{\psi}_1$ are

$$\left.\begin{aligned}
\psi_{1r}(r,\theta,\varphi,t)&=\sum_n \frac{l(l+1)}{r^2}\Psi_1(r)Y_l^m(\theta,\varphi)e^{\zeta_n t}\\
\psi_{1\theta}(r,\theta,\varphi,t)&=\sum_n \frac{1}{r}\frac{d\Psi_1(r)}{dr}\frac{\partial Y_l^m(\theta,\varphi)}{\partial\theta}e^{\zeta_n t}\\
\psi_{1\varphi}(r,\theta,\varphi,t)&=\sum_n \frac{1}{r\sin\theta}\frac{d\Psi_1(r)}{dr}\frac{\partial Y_l^m(\theta,\varphi)}{\partial\varphi}e^{\zeta_n t}
\end{aligned}\right\}, \tag{B7}$$

with

$$\Psi_1(r)=D_n r^{1/2} J_{l+1/2}(is_n r), \tag{B8}$$

where $J_{l+1/2}$ is the spherical Bessel function of order $l+1/2$ and $s_n=\sqrt{\zeta_n/\nu_1}$.

The coefficients B_n and D_n are determined by substituting Eqs. (B6) and (B7) into the kinematic boundary condition (A5) and the tangential stress balance condition (A10) and (A11),

$$\left.\begin{aligned}
B_n&=\frac{\eta_n\zeta_n}{l r_0^{l-1}}\left[1+\frac{2\left(l^2-1\right)}{2xQ_{l+1/2}(x)-x^2}\right]\\
D_n&=-\frac{2(l-1)\eta_n\zeta_n r_0^{3/2}}{l\left[2xJ_{l+3/2}(x)-x^2J_{l+1/2}(x)\right]}
\end{aligned}\right\}, \tag{B9}$$

where $Q_{l+1/2}(x)=J_{l+3/2}(x)/J_{l+1/2}(x)$ and $x=is_n r_0$.

It is noticeable that the presence of the time-dependent term $\cos(\Omega t)$ in Eq. (B3) makes the equation inhomogeneous in time and couples the different Fourier modes n considering the Floquet form of the surface disturbance η as Eqs. (A12) and (A13), which leads to

$$\begin{aligned}
\cos(\Omega t)\eta_l^m(t)&=\frac{e^{i\Omega t}+e^{-i\Omega t}}{2}\sum_n \eta_n e^{[\beta+i(\gamma+n\Omega)]t}\\
&=\frac{1}{2}\sum_n(\eta_{n-1}+\eta_{n+1})e^{\zeta_n t}.
\end{aligned} \tag{B10}$$

Substituting Eqs. (B6) and (B9) into Eq. (B3) and with the recurrence relation (B10), we obtain the pressure on the interface on the inner side of the droplet

$$\begin{aligned}
p_1|_{r=r_0+\eta}=&-\sum_{l=0}^{+\infty}\sum_{m=0}^{l}\sum_{n=0}^{+\infty}\frac{\rho_1\eta_n\zeta_n^2 r_0}{l}\left[1+\frac{2\left(l^2-1\right)}{2xQ_{l+1/2}(x)-x^2}\right]e^{\zeta_n t}Y_l^m\\
&+\frac{1}{2}\rho_1 A_0\sum_{l=0}^{+\infty}\sum_{m=0}^{l}\sum_{n=0}^{+\infty}(\eta_{n-1}+\eta_{n+1})e^{\zeta_n t}Y_l^m+\rho_1 A_0\cos(\Omega t)r_0+C_1.
\end{aligned} \tag{B11}$$

If the inviscid fluid outside the droplet is initially irrotational, it will remain so. Consequently, a velocity potential ϕ_2 satisfying $\boldsymbol{u}_2=\nabla\phi_2$ can be introduced to the continuity equation (A3), yielding

$$\nabla^2\phi_2=0. \tag{B12}$$

Integrating Eq. (A4) over the radial direction leads to

$$p_2=-\rho_2\frac{\partial\phi_2}{\partial t}+\rho_2 A_0\cos(\Omega t)r+C_2(t), \tag{B13}$$

where $C_2(t)$ is another integral constant as a function of t.

Considering the natural boundary condition that the velocity is finite at $r=\infty$ and the kinematic boundary condition (A5), we have the solution to Eq. (B12) as

$$\phi_2=-\sum_n \eta_n\frac{\zeta_n r_0}{l+1}\left(\frac{r}{r_0}\right)^{-(l+1)}e^{\zeta_n t}Y_l^m \tag{B14}$$

for a given spherical harmonic $Y_l^m(\theta,\varphi)$. Substituting Eq. (B14) into Eq. (B13) and with the recurrence relation (B10), we have the pressure on the interface at the outer side of the droplet

$$\begin{aligned}
p_2|_{r=r_0+\eta}=&\sum_{l=0}^{+\infty}\sum_{m=0}^{l}\sum_{n=0}^{+\infty}\frac{\rho_2\eta_n\zeta_n^2 r_0}{l+1}e^{\zeta_n t}Y_l^m\\
&+\frac{1}{2}\rho_2 A_0\sum_{l=0}^{+\infty}\sum_{m=0}^{l}\sum_{n=0}^{+\infty}(\eta_{n-1}+\eta_{n+1})e^{\zeta_n t}Y_l^m\\
&+\rho_2 A_0\cos(\Omega t)r_0+C_2.
\end{aligned} \tag{B15}$$

[1] M. Faraday, "On a peculiar class of acoustical figures; and on certain forms assumed by groups of particles upon vibrating elastic surfaces," Philos. Trans. R. Soc. London **121**, 299–340 (1831).

[2] J. Miles and D. Henderson, "Parametrically forced surface waves," Annu. Rev. Fluid. Mech. **22**, 143–165 (1990).

[3] A. J. Archer, A. M. Rucklidge, and E. Knobloch, "Quasicrystalline order and a crystal-liquid state in a soft-core fluid," Phys. Rev. Lett. **111**, 165501 (2013).

[4] P. Chen and J. Viñals, "Pattern selection in Faraday waves," Phys. Rev. Lett. **79**, 2670 (1997).

[5] L. Kahouadji, N. Perinet, L. S. Tuckerman, S. Shin, J. Chergui, and D. Juric, "Numerical simulation of supersquare patterns in Faraday waves," J. Fluid Mech. **772**, R2 (2015).

[6]M.-T. Westra, D. J. Binks, and W. Van De Water, "Patterns of Faraday waves," J. Fluid Mech. **496**, 1–32 (2003).
[7]L. Daudet, V. Ego, S. Manneville, and J. Bechhoefer, "Secondary instabilities of surface waves on viscous fluids in the Faraday instability," Europhys. Lett. **32**, 313–318 (1995).
[8]A. Kityk, J. Embs, V. Mekhonoshin, and C. Wagner, "Spatiotemporal characterization of interfacial Faraday waves by means of a light absorption technique," Phys. Rev. E **72**, 036209 (2005).
[9]A. Kudrolli and J. Gollub, "Patterns and spatiotemporal chaos in parametrically forced surface waves: A systematic survey at large aspect ratio," Physica D **97**, 133–154 (1996).
[10]X. Ma, B. Huang, Y. Li, Q. Chang, S. Qiu, Z. Su *et al.*, "Numerical simulation of single bubble dynamics under acoustic travelling waves," Ultrason. Sonochem. **42**, 619–630 (2018).
[11]T. Donnelly, J. Hogan, A. Mugler, N. Schommer, M. Schubmehl, A. J. Bernoff *et al.*, "An experimental study of micron-scale droplet aerosols produced via ultrasonic atomization," Phys. Fluids **16**, 2843–2851 (2004).
[12]C. Goodridge, H. Hentschel, and D. Lathrop, "Breaking Faraday waves: Critical slowing of droplet ejection rates," Phys. Rev. Lett. **82**, 3062–3065 (1999).
[13]R. J. Lang, "Ultrasonic atomization of liquids," J. Acoust. Soc. Am. **34**, 6–8 (1962).
[14]Y. K. Li and A. Umemura, "Threshold condition for spray formation by Faraday instability," J. Fluid Mech. **759**, 73–103 (2014).
[15]V. Akkerman and C. K. Law, "Coupling of harmonic flow oscillations to combustion instability in premixed segments of triple flames," Combust. Flame **172**, 342–348 (2016).
[16]V. Bychkov, "Analytical scalings for flame interaction with sound waves," Phys. Fluids **11**, 3168–3173 (1999).
[17]G. Searby and D. Rochwerger, "A parametric acoustic instability in premixed flames," J. Fluid Mech. **231**, 529–543 (1991).
[18]L. Matthiessen, "Akustische versuche die kleinsten transversalwellen der flüssigkeiten betreffend," Ann. Phys. Chem. **210**, 107–117 (1868).
[19]T. B. Benjamin and F. Ursell, "The stability of the plane free surface of a liquid in vertical periodic motion," Proc. R. Soc. A **225**, 505–515 (1954).
[20]W. Eisenmenger, "Dynamic properties of the surface tension of water and aqueous solutions of surface active agents with standing capillary waves in the frequency range from 10 kc/s to 1.5 Mc/s," Acta Acustica united with Acustica **9**, 327–340 (1959).
[21]S. Ciliberto and J. P. Gollub, "Phenomenological model of chaotic mode competition in surface waves," Il Nuovo Cimento D **6**, 309–316 (1985).
[22]K. Kumar and L. S. Tuckerman, "Parametric instability of the interface between two fluids," J. Fluid Mech. **279**, 49–68 (1994).
[23]K. Kumar, "Linear theory of Faraday instability in viscous liquids," Proc. R. Soc. A **452**, 1113–1126 (1996).
[24]W. S. Edwards and S. Fauve, "Parametrically excited quasicrystalline surface waves," Phys. Rev. E **47**, R788–R791 (1993).
[25]S. Fauve, K. Kumar, C. Laroche, D. Beysens, and Y. Garrabos, "Parametric instability of a liquid-vapour interface close to the critical point," Phys. Rev. Lett. **68**, 3160–3163 (1992).
[26]S. Schmidt, O. Krüger, K. Göckeler, and C. O. Paschereit, "Numerical investigation of the breakup behavior of an oscillating two-phase jet," Phys. Fluids **30**, 072101 (2018).
[27]V. G. Kozlov, S. V. Subbotin, and R. R. Sabirov, "Steady flows in deformed elastic sphere subject to rotational oscillations," Phys. Fluids **30**, 093606 (2018).
[28]D. Kang, A. Nadim, and M. Chugunova, "Marangoni effects on a thin liquid film coating a sphere with axial or radial thermal gradients," Phys. Fluids **29**, 072106 (2017).
[29]P. Capobianchi, M. Lappa, and M. S. N. Oliveira, "Walls and domain shape effects on the thermal Marangoni migration of three-dimensional droplets," Phys. Fluids **29**, 112102 (2017).
[30]A. Ponce-Torres, M. A. Herrada, J. M. Montanero, and J. M. Vega, "Linear and nonlinear dynamics of an insoluble surfactant-laden liquid bridge," Phys. Fluids **28**, 112103 (2016).
[31]N. Barai and N. Mandal, "Breakup modes of fluid drops in confined shear flows," Phys. Fluids **28**, 073302 (2016).
[32]Lord Rayleigh, "On the capillary phenomena of jets," Proc. R. Soc. London **29**, 71–97 (1879).
[33]S. Chandrasekhar, *Hydrodynamic and Hydromagnetic Stability* (Clarendon Press, Oxford, 1961).
[34]G. Terrones and M. D. Carrara, "Rayleigh-Taylor instability at spherical interfaces between viscous fluids: Fluid/vacuum interface," Phys. Fluids **27**, 054105 (2015).
[35]A. James, B. Vukasinovic, M. K. Smith, and A. Glezer, "Vibration-induced drop atomization and bursting," J. Fluid Mech. **476**, 1–28 (2003).
[36]M. Okada and M. Okada, "Observation of the shape of a water drop on an oscillating Teflon plate," Exp. Fluids **41**, 789–802 (2006).
[37]B. Vukasinovic, M. K. Smith, and A. Glezer, "Mechanisms of free-surface breakup in vibration-induced liquid atomization," Phys. Fluids **19**, 012104 (2007).
[38]F. Liu, N. Kang, Y. Li, and Q. Wu, "Experimental investigation on the spray characteristics of a droplet under sinusoidal inertial force," Fuel **226**, 156–162 (2018).
[39]F. Liu, N. Kang, Y. Li, and Q. Wu, "Experimental investigation on the atomization of a spherical droplet induced by Faraday instability," Exp. Therm. Fluid Sci. **100**, 311–318 (2019).
[40]C. L. Shen, W. J. Xie, and B. Wei, "Parametrically excited sectorial oscillation of liquid drops floating in ultrasound," Phys. Rev. E **81**, 046305 (2010).
[41]A. Qi, L. Y. Yeo, and J. R. Friend, "Interfacial destabilization and atomization driven by surface acoustic waves," Phys. Fluids **20**, 074103 (2008).
[42]M. K. Tan, J. R. Friend, O. K. Matar, and L. Y. Yeo, "Capillary wave motion excited by high frequency surface acoustic waves," Phys. Fluids **22**, 112112 (2010).
[43]A. H. Ebo Adou and L. S. Tuckerman, "Faraday instability on a sphere: Floquet analysis," J. Fluid Mech. **805**, 591–610 (2016).
[44]B. A. Puthenveettil and E. Hopfinger, "Evolution and breaking of parametrically forced capillary waves in a circular cylinder," J. Fluid Mech. **633**, 355 (2009).
[45]E. Y. Harper, G. W. Grube, and I. D. Chang, "On the breakup of accelerating liquid drops," J. Fluid Mech. **52**, 565–591 (1972).
[46]H. Lamb, *Hydrodynamics* (Cambridge University Press, 1932).
[47]C. L. Goodridge, W. T. Shi, H. Hentschel, and D. P. Lathrop, "Viscous effects in droplet-ejecting capillary waves," Phys. Rev. E **56**, 472–475 (1997).
[48]E. T. Copson, *Asymptotic Expansions* (Cambridge University Press, 2004).
[49]B. Vukasinovic, M. K. Smith, and A. Glezer, "Spray characterization during vibration-induced drop atomization," Phys. Fluids **16**, 306–316 (2004).
[50]E. Meron, "Parametric excitation of multimode dissipative systems," Phys. Rev. A **35**, 4892–4895 (1987).
[51]P. Pedersen, "Stability of the solutions to Mathieu-Hill equations with damping," Ing.-Arch. **49**, 15–29 (1980).
[52]L. Turyn, "The damped Mathieu equation," Q. Appl. Math. **51**, 389–398 (1993).
[53]M. Majumder, C. Rendall, M. Li, N. Behabtu, J. A. Eukel, R. H. Hauge *et al.*, "Insights into the physics of spray coating of SWNT films," Chem. Eng. Sci. **65**, 2000–2008 (2010).
[54]M. S. Plesset and C. G. Whipple, "Viscous effects in Rayleigh-Taylor instability," Phys. Fluids **17**, 1–7 (1974).
[55]L. Kelvin, "XLVI. Hydrokinetic solutions and observations," London Edinburgh Dublin Philos. Mag. J. Sci. **42**, 362–377 (1871).